THERMAL AND STABILITY CONSIDERATIONS OF CANDU-SCWR SLIDING PRESSURE STARTUP

Junjie Pan, Jianqiang Shan
School of Nuclear Science and Technology,
Xi'an Jiaotong University, Xi'an China 710049

Abstract

The feasibility of the sliding pressure startup of CANDU-SCWR is assessed from both thermal and stability considerations. The coupled neutronic/thermal-hydraulics stabilities are investigated for both super- and sub-critical pressure operating conditions. The startup system and startup procedure are designed. The detailed thermal-hydraulics analysis is assessed based on the subchannel analysis and a stability map is constructed based on non-dimensional parameters and frequency domain method. The results show that the maximum cladding surface temperature can be well restricted lower than criterion (850℃), and the stability can be maintained by controlling the power and flow rate during startup.

1. Introduction

The supercritical water cooled reactor (SCWR), recognized as one of the Generation IV reactor concepts, has been conceptually studied by Japan, Canada, EU, USA and other countries since 1989 [1]. SCWRs have been designed based on the abundant experiences of water cooled reactors (LWR/PHWR) and supercritical fossil-fired power plants (FPP). SCWRs are aimed for high thermal efficiency and reduced material expenditure, by high steam temperature and pressure, and compact plant system.

There are mainly two types of SCWR concepts [2]: (a) a large reactor pressure vessel containing the reactor core (fuelled), analogous to conventional PWRs and BWRs, and (b) distributed pressure tubes or channels containing fuel bundles, analogous to conventional CANDU and RBMK nuclear reactors.Table 1 summarizes the salient design parameters of the CANDU-SCWR.

Table 1 CANDU-SCWR preliminary specifications

Parameter	Value	Parameter	Value
Spectrum	Thermal	Thermal power (MW)	2540
Electric power (MW)	1220	Thermal efficiency (%)	48
Inlet temperature (◦C)	350	Outlet temperature (◦C)	625
Flowrate (kg/s)	1320	Calandria diameter (m)	4
Fuel	UO2/Th	Enrichment (%)	4
Number of fuel channels	300	Number of fuel elements	43 or 61
Cladding material	Ni alloy	Limiting cladding temperature (◦C)	850
Moderator	Heavy water	Coolant	Light water

The SCWRs have higher operating pressure and temperature, and the thermo-physical properties and transport properties of the coolant in the core will change largely during the transition from subcritical pressure to supercritical pressure. So the startup system of SCWRs is different from that of subcritical water cooled reactors.Compared to constant pressure startup system, the sliding pressure startup system (Figure 1) do not need complicated valve operations, and the pumping power consumption is decreased, which results in a higher efficiency during low-load operations. Therefore, the sliding pressure startup procedure is usually applied in SCWR system.

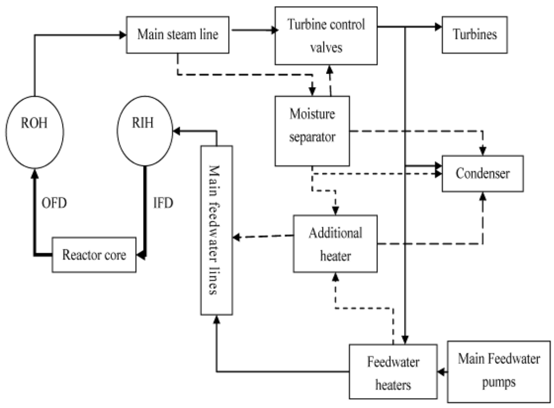

Dashed line: startup flow chart

Solid line: normal operation flow chart

Figure 1 Sliding pressure startup system for CANDU-SCWR

The thermal analysis of the startup of a low-temperature supercritical-pressure light water cooled fast reactor (SCFR) was carried out by Nakatsuka et al. [3]. In their studies, the feasibilities of both constant pressure startup system and sliding pressure startup system for SCFR were investigated from the viewpoint of thermal considerations. Detailed analyses of various startup phases were not carried out in their study. Yi et al. [4] analyzed the SCLWR-H with detailed thermal-hydraulic analyses with single channel model. Phases such as pressurization phase and temperature-raising phase were investigated and analyzed. The required detailed procedures for these phases were proposed.

In US reference SCWR design, sliding pressure startup was chosen and the startup procedures have been investigated by Zhao [5]. The low coolant flow rate and large density change in the core may cause undesirable flow instabilities in the fuel channels, and flow instabilities in reactor can disturb the control and the operation of the reactor, so careful design and analysis must be done to ensure that these instabilities can be detected. The instability types in the BWR can be categorized into static and dynamic instabilities. The three static instability types are: flow excursion (Ledinegg) instability, flow regime "relaxation" instability and geysering type instability; the four dynamic instability types are: density wave oscillations, pressure drop oscillations, flow regime-induced instability and acoustic instability. Because the dynamics of CANDU-SCWR is similar to that of BWR, so the instabilities in

CANDU-SCWR can be subject to the same types of instabilities in BWR. This study will consider only density wave instability, which is the most important instability type in reactor design.

For boiling channels, density-wave oscillations (DWO) have been research in the last ten years. Kakac et al. [6] gave a review of two-phase flow dynamic instabilities in tube boiling systems. Yi et al. [7] carried out linear analyses on the flow stability of supercritical pressure light water reactors to investigate the thermal-hydraulic phenomena in an upward flowing heated channel as well as coupled nuclear/thermal-hydraulic in- stabilities, the effects of water rods also be took into account.

Shan et al [8] carried out detailed subchannel analysis for CANDU-SCWR sliding pressure startup procedures with ATHAS code. The sliding pressure startup curves are illustrated in: (1) Start of Reactor Core at Subcritical Pressure; (2) Start of Turbine; (3) Pressurization Phase; (4) Feedwater Temperature Increasing Phase; and (5) Core Power Increasing Phase, which is shown in Figure 2.The calculation results show that during these phases, the maximum cladding temperature satisfies well the criterion.

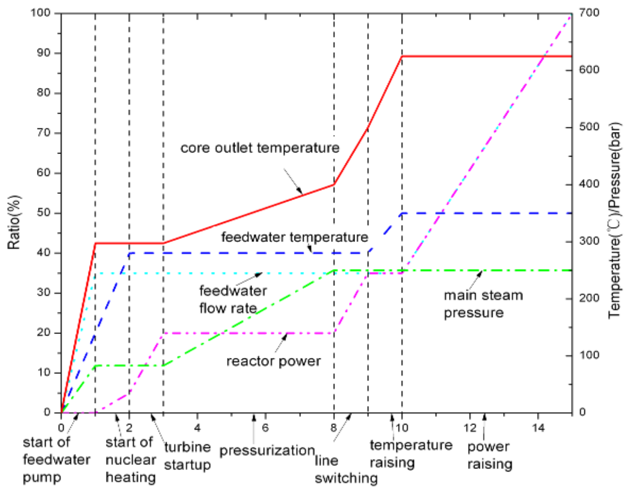

Figure 2 Sliding pressure startup curve (by thermal analyse)

2. stability Analysis of CANDU- SCWR startup

During sliding pressure startup, the reactor should operate at supercritical pressure[8] and subcritical pressure, and the density of coolant will have significant change while the temperature crosses the pseudo-critical point or saturated line, the three-region model is chosen. A stability map that defines the onset of DWO instabilities has been constructed based on non-dimensional parameters and frequency domain method.

2.1 Three-region model

Although there is no phase change in supercritical pressure, the coolant thermal and transport properties such as density, specific heat, dynamic viscosity, thermal conductivity, etc. have drastic change at pseudo-critical region. Homogenous Equilibrium Model (HEM) is used because the two fluids are well coupled at such high pressure. Therefore, the three region model (Figure 3): (1) a region for the "heavy fluid" with constant density, (2) a region of a mixture of "heavy" and "light" fluids similar to a homogeneous- equilibrium two-phase mixture, and finally (3) a region for the "light fluid" which behaves like an ideal gas or superheated steam are used for stability analysis.

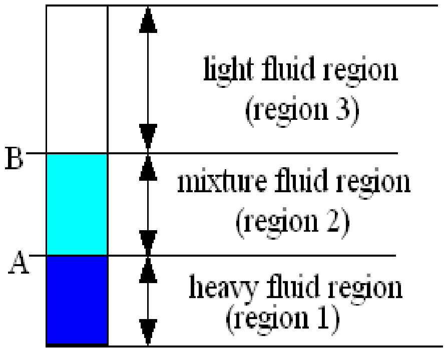

Figure 3 Supercritical water simulated by three-region model

The boundary between region 1 and region 2 is defined at the temperature T_A = 350°C for all of the supercritical states, The boundary between region 2 and 3 is defined at temperature T_B which was calculated by Zhao [5].

2.2 Derivation of nondimensional parameters

The nondimensional parameters for two phase flow instability at subcritical pressure were the Subcooling Number and the Phase Change Number which is governed by Ishii and Zuber[9]. The Subcooling Number was defined as:

$$N_{sub} = \frac{(h_f - h_{in})}{h_{fg}} \frac{\rho_f - \rho_g}{\rho_g} \tag{1}$$

The Phase Change Number was defined as:

$$N_{pch} = \frac{v_{fg}}{h_{fg}} \frac{q'' P_h}{A_c} \frac{L}{u_{in}} \tag{2}$$

Similar to the subcritical system, it is proposed that the governing parameters for the supercritical system are a Pseudo-subcooling Number and an Expansion Number, which have been defined by Zhao[5].

$$N_{psub} = \frac{(h_A - h_{in})}{h_{AB}} \frac{\rho_A - \rho_B}{\rho_B} \tag{3}$$

$$N_{\exp} = \frac{R}{pc_p} \frac{q'' P_h}{A_c} \frac{L}{u_{in}} \tag{4}$$

Points A and B are the same as defined in the three-region model. R is ideal gas constant and

2.3 Derivation of the characteristic equation

During density wave oscillations, the fuel rods are coupled with the coolant thermal-hydraulic dynamics through the fuel rods heat flux dynamics. To investigate the fuel dynamics effects on single channel stability, a coupled neutronic/ thermal-hydraulic stability model was developed based on the coolant thermal-hydraulics model, fuel rod heat transfer model and point neutronic kinetics model. The coupled neutronic/thermal-hydraulic stability model is shown in Figure 4.

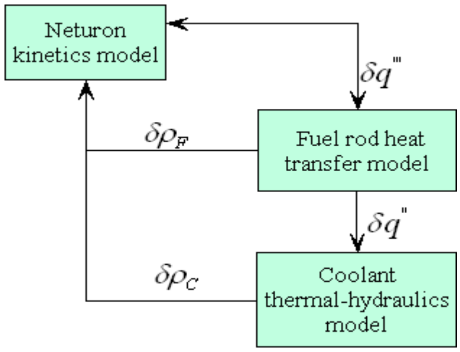

Figure 4 coupled neutronic thermal-hydraulic stability models

2.3.1. Neutron Kinetics Model

$$\begin{cases} \dfrac{\partial n(t)}{\partial t} = \dfrac{\rho(t)-\beta}{\Lambda} n(t) + \sum_{i=1}^{6} \lambda_i C_i(t) \\ \dfrac{\partial C_i(t)}{\partial t} = \dfrac{\beta_i}{\Lambda} n(t) - \lambda_i C_i(t) \end{cases} \tag{5}$$

The reactivity in point kinetics equations depends on the change of fuel temperature and coolant temperature, α_f is the reactivity coefficient of fuel temperature and α_{cool} are the reactivity coefficient of coolant temperature, which was given in[10].

$$\partial\rho(s) = \alpha_f \delta\overline{T_f(s)} + \alpha_{cool}\delta T_{cool}(s) \tag{6}$$

The $\delta q'''$ in Figure 4 can be define as：

$$\delta q'''(s) = \frac{2q''}{R_1}\frac{1}{\Lambda s}\frac{1}{1+\dfrac{1}{\Lambda}\sum_{i=1}^{6}\dfrac{\beta_i}{s+\lambda_i}} * (\alpha_f \delta\overline{T_f(s)} + \alpha_{cool}\delta T_{cool}(s)) \tag{7}$$

The delayed neutron data for SCLWR-H is given in Table 2

Table 2 Delayed neutron data for thermal fission of U^{235} in SCLWR-H

Group	Effective delayed neutron decay constant (λ_i) (s^{-1})	Effective delayed neutron fraction (β_i)
1.	0.01271596	0.0002432
2.	0.03173751	0.0013632
3.	0.11552453	0.0012032
4.	0.3108028	0.0026048
5.	1.39747415	0.0008192
6.	3.87233068	0.0001664
Total delayed neutron fraction		0.0064
Prompt neutron generation time		0.000043 s

2.3.2. Fuel Rod Heat Transfer Model

A fuel rod heat transfer model is shown in Figure 5, which includes fuel pellet, gas gap and cladding. The temperature distribution can be calculated from the follow equations.

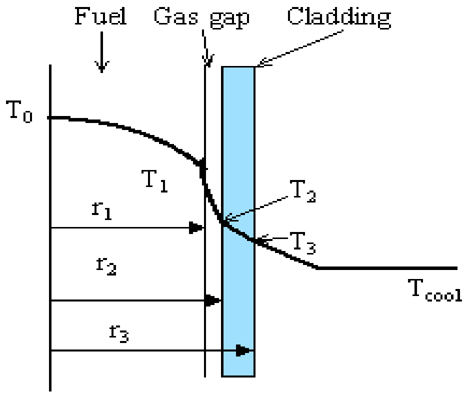

Figure 5 Fuel Rod Heat Transfer Model

$$\frac{\partial}{\partial t}(\rho_f C_p T_f) = \frac{1}{r}\cdot\frac{\partial}{\partial r}(rk_f \frac{\partial T_f}{\partial r}) + q''' \tag{8}$$

The boundary conditions are given by:

$$\begin{cases} \left.\frac{\partial T_f}{\partial r}\right|_{r=0} = 0 \\ q'''(r_f, t) = -k_f(T_f)\left.\frac{\partial T_f}{\partial r}\right|_{r=r_f} \end{cases} \tag{9}$$

$\overline{T_f}$ is the average temperature of the fuel pellet which can be defined as

$$\overline{T_f} = \frac{\int_0^{r_1} 2\pi r_f T_f dr}{\pi r_1^2} \tag{10}$$

The heat transfer equation from the fuel cladding surface to the coolant is given as:

$$q'' = \overline{h}(T_3 - T_{cool}) \tag{11}$$

After perturbing and Laplace transformation the above formulas, the equation (12) is given. In this equation, $\delta q'''$ which means the change of core power can be given by Neutron Kinetics Model, and it is shown in equation (7).

$$[\frac{1}{\overline{h}} + \frac{1}{s(\rho c_p)_f}\cdot\frac{2r_3}{r_1^2} + r_3(\frac{1}{4k_f} + \frac{\ln\frac{r_2}{r_1}}{k_g} + \frac{\ln\frac{r_3}{r_2}}{k_c})]\delta q'' = \frac{q''}{\overline{h}}\frac{\delta\overline{h}}{\overline{h}} + \frac{\delta q'''}{s(\rho c_p)_f} - \frac{\delta h_\infty}{c_{p,\infty}} \tag{12}$$

2.3.3. Fuel Channel Thermal-Hydraulic Model

The Fuel Channel Thermal-Hydraulic Model mainly includes the conservation equations of mass, energy and momentum and the state equation for the coolant channel.

Mass Conservation:

$$\frac{\partial \rho}{\partial t}+\frac{\partial \rho u}{\partial z}=0 \tag{13}$$

Energy Conservation:

$$\frac{\partial(\rho h)}{\partial t}+\frac{\partial(\rho u h)}{\partial z}=\frac{P_h}{Ac}q^{"} \tag{14}$$

Momentum Conservation:

$$\frac{\partial \rho u}{\partial t}+\frac{\partial(\rho u^2)}{\partial z}=-\frac{\partial \rho}{\partial z}-\rho g-\frac{f}{D_e}\frac{\rho u^2}{2} \tag{15}$$

State Equation:

$$\rho = p(P,h) \tag{16}$$

2.4 Characteristic Equation

The characteristic equation for CANDU-SCWR single channel stability was derived from the momentum, energy and mass conservation equations. A uniformly distributed constant fuel surface heat flux is applied. The single flow channel of the SCWR core is divided into four parts, which is the inlet orifice, the inlet non-heated part, the heated part and the outlet non-heated part.

(1) Inlet orifice

The momentum equation for the inlet orifice can be expressed as:

$$\Delta p_{ori}=k_{in}\frac{\rho_A u_{in}{}^2}{2} \tag{17}$$

Perturbation and Laplace transformation of the above equation yields:

$$\delta\Delta p_{ori}=k_{in}\rho_A u_{in}\delta u_{in} \tag{18}$$

(2) Heated part

The heated part at supercritical pressure systerm includes "heavy fluid" region, "Heavy and light fluid mixture" region and "Light fluid" region.

(2-A) "Heavy fluid" region

$$\rho_A\frac{\partial h}{\partial t}+\rho_A u_{in}\frac{\partial h}{\partial z}=\frac{q^{"}P_h}{A_c} \tag{19}$$

$$-\frac{\partial p}{\partial z}=\rho_A\frac{\partial u_{in}}{\partial t}+\frac{f_1\rho_A u_{in}^2}{2De}+\rho_A g \tag{20}$$

The energy Equation and the momentum conservation equation are integrated, perturbed and Laplace transformed.

$$\delta\Delta p_1(s)=\int_0^{\lambda_1}(\rho_A\frac{d(\delta u_{in})}{dt}+\frac{f_1\rho_A u_{in}\delta u_{in}}{De})dz+(\frac{f_1\rho_A u_{in}^2}{2De}+\rho_A g)\delta\lambda_1(s) \tag{21}$$

$$\delta\Delta p_1(s)=\Gamma_1\delta u_{in}+\Delta_1\delta h_{in} \tag{22}$$

Use the same method, characteristic equations at "Heavy and light fluid mixture" region and "Light fluid" region are expressed as follows.

(2-B) "Heavy and light fluid mixture" region

$$\begin{aligned}\delta\Delta p_2 &= \int_{\lambda_1}^{\lambda_2}[(s+\Omega_1)\rho_m + \frac{f_2 G}{2De}]\delta u_m dz + \int_{\lambda_1}^{\lambda_2}[(s+\Omega_1)u_m + \frac{f_2 u_m{}^2}{2De} + g]\delta\rho_m dz \\ &-(G\Omega_1 + \frac{f_2 G}{2De}u_{in} + \rho_f g)\delta\lambda_1 + (G\Omega_1 + \frac{f_2 G}{2De}u_m(\lambda_2) + \rho_g g)\delta\lambda_2 \\ &= \Gamma_2\delta u_{in} + \Delta_2\delta h_{in}\end{aligned} \tag{23}$$

(2-C) "Light fluid" region

$$\begin{aligned}\delta(\Delta p_3) &= \int_{\lambda_2}^{L}[(s+\Omega_2)\rho + \frac{f_3}{D_e}G]\delta u dz + \int_{\lambda_2}^{L}[(s+\Omega_2)u + \frac{f_3}{2D_e}u^2]\delta\rho dz \\ &-(G\Omega_2 + \frac{f_3}{2D_e}Gu_m(\lambda_2) + \rho_g G)\delta\lambda_2 \\ &= \Gamma_3\delta u_{in} + \Delta_3\delta h_{in}\end{aligned} \tag{24}$$

(3) Non-heated part

The Non-heated part includes inlet part and outlet part.

$$\delta\Delta p_{in} = (\frac{f_1}{D_e L_{in} G} + s\rho_A L_{in})\delta u_{in} \tag{25}$$

$$\begin{aligned}\delta\Delta p_{out} &= (\frac{f_3}{D_e L_{out}}\frac{u(L)^2}{2} + gL_{out} + su(L)L_{out})\delta\rho(L) + (\frac{f_3}{D_e L_{in} G} + s\rho(L)L_{out})\delta u(L) \\ &= \Gamma_4\delta u_{in} + \Delta_4\delta h_{in}\end{aligned} \tag{26}$$

From the above, the perturbation of the total channel pressure can be expressed as:

$$\begin{aligned}\delta\Delta p_{total} &= \delta\Delta p_{ori} + \delta\Delta p_{in} + \delta\Delta p_1 + \delta\Delta p_2 + \delta\Delta p_3 + \delta\Delta p_{out} \\ &= \Pi_1\delta u_{in} + \Pi_2\delta h_{in}\end{aligned} \tag{27}$$

$$\Pi_1 = f(Geometry, p, u_{in}, s, h_{in}, q^{"}) = 0 \tag{28}$$

3. Stability map construction

For a specific heated channel, the geometry is specified. If the system pressure and inlet flow rate are also specified, the remaining variables for the characteristic equation are: complex variable $s = \sigma + j\omega$, coolant inlet enthalpy hin, and surface heat flux q". The stability of the system depends on the value of σ . For the system to be stable, all the poles of the closed loop transfer function must have negative real parts (σ <0).

$$DR = \frac{u(t_2)}{u(t_1)} = \exp(-2\pi\frac{\|\sigma\|}{\|\omega\|}) \tag{29}$$

The neutral stability boundary or the stability map is formed by the points where DR=1 and it can construct by the procedure:

(A)Setting boundary value $s=j\omega$.

(B)Giving a specific h_{in}, then solving the system of equations to get q'', ω .

$$\begin{cases} \mathrm{Re}(\Pi_1(q'',\omega)) = 0 \\ \mathrm{Im}(\Pi_1(q'',\omega)) = 0 \end{cases} \tag{30}$$

Using h_{in} and q" to calculate N_{psch} and N_{exp}.

(C) Repeating procedure (B) by changing h_{in}, the other boundary pairs of h_{in} and q" are obtained.

(D) Plotting the results on $N_{psch} – N_{exp}$ plane.

This procedure is made by MATLAB, which can plot simple stability maps.

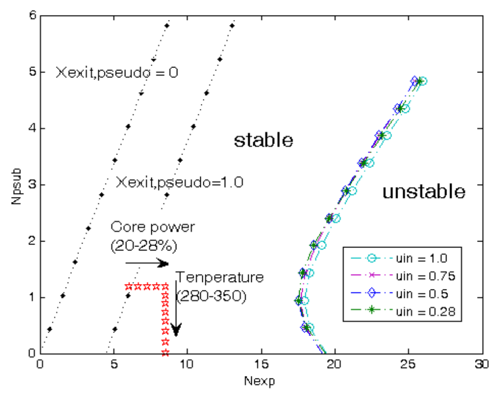

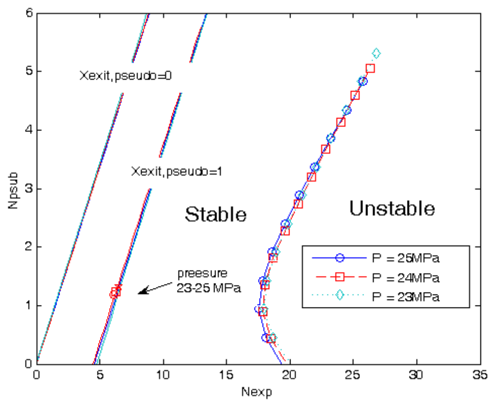

Figure 6 stability map at 25 MPa

Figure 7 stability map at 23-25MPa

The stability maps at supercritical pressure are shown in Figure 6 and Figure 7From the figs, the inlet flow rate and system pressure have not much effect on the stability boundary in the Pseudo Subcooling Number and Expansion Number plane. The red points which denote startup parameters show that startup phase in Figure 2 is stable at supercritical pressure.

The method to get stability map at subcritical pressure is similar to the method at supercritical pressure. In this study, the HEM model is chosen for simple and conservative result.

The stability maps at the subcritical pressure in Figure 8 also show that subcritical pressure has not much effect on the stability boundary. The triangular points show that increasing core power at the same pressure makes the system unstable, and the other points show that increasing pressure at the same power makes the system stable. Since there are some startup points in unstable region, it can conclude that startup phase at subcritical pressure is unstable.

The Figure 6,7 and 8 also show that the same system in supercritical pressure region has more stable margin than subcritical region. The mix-phases in subcritical region may not be stable especially at low pressure region. This is because the gas phase which makes the system unstable will appear early and has more volume at low pressure region.

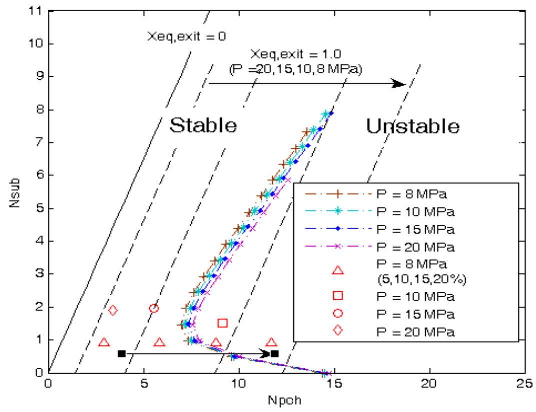

Figure 8 stability map at subcritical pressure

4. Thermal-Hydraulic and Stability Analysis of CANDU-SCWR

Since startup phase at subcritical pressure is unstable, the sliding pressure startup curve must be remodifed to adapt both thermal-hydraulic and stability considerations.

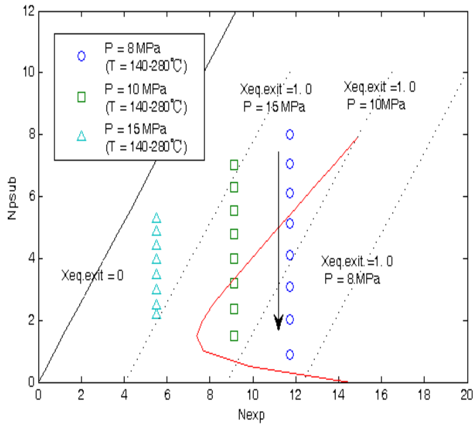

Figure 9 stability analysis for different temperature

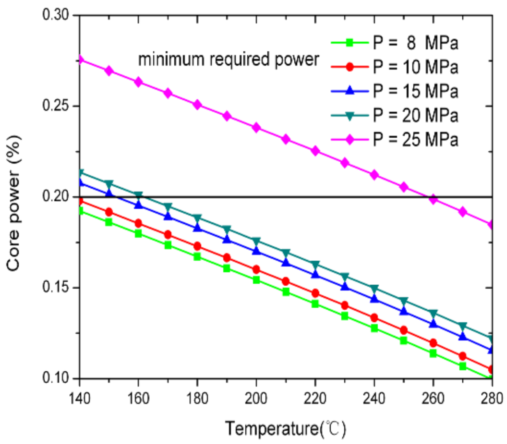

Figure 10 thermal analysis for different temperature

Form Figure 9, decreasing the coolant temperature makes the system stable. Obviously, it also makes the maximum cladding temperature lower. But if the temperature is too low, the minimum required power must be greater than the startup power 20% to make sure the minimum required core exit quality in subcritical pressure condition and fixed exit enthalpy in supercritical pressure satisfy the criterion (Figure 10). So the pressurization phase should divide into three parts:(1) pressurization from 8.3MPa to 15MPa when the feedwater temperature is 160°C; (2) keep the pressure at 15MPa, increase the feedwater temperature from 160°C to 280°C; (3) pressurization from 15MPa to 25MPa. The new curve is shown in Figure 11. The thermal show that the maximum cladding temperature satisfies well the criterion.

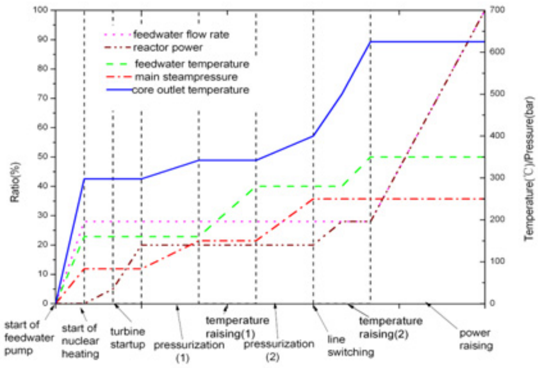

Figure 11 Sliding pressure startup curve

The Figure 12 is the thermal analysis during startup by ATHAS code, it shown that the maximum cladding temperature satisfies well the criterion.

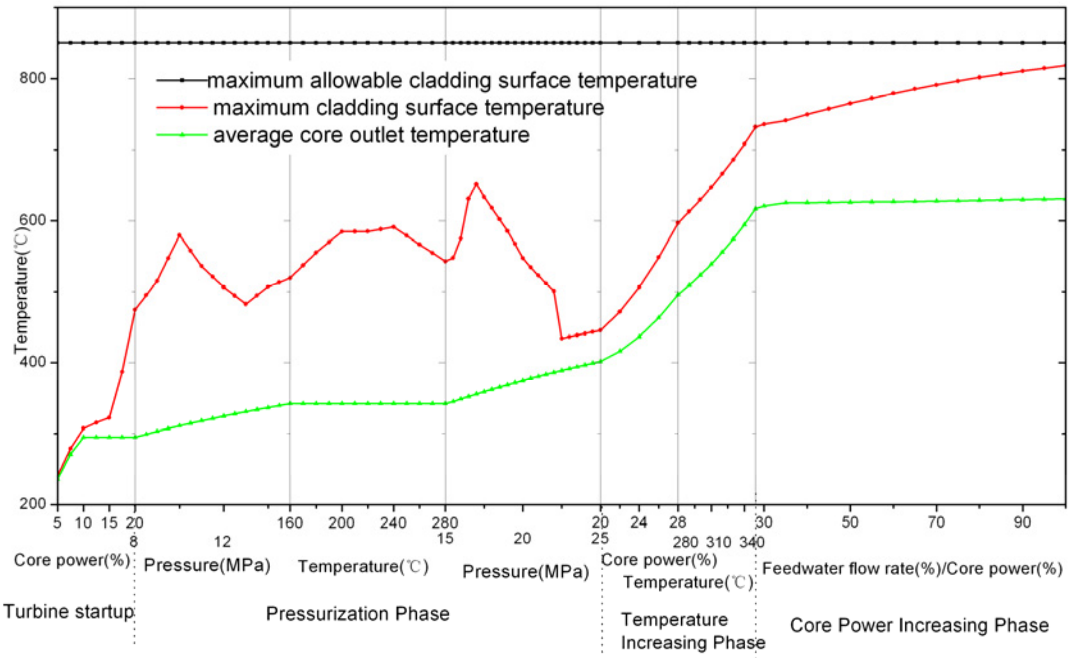

Figure 12 thermal analysis during startup

After the modification, startup phase at subcritical pressure will be stable (Figure 13).

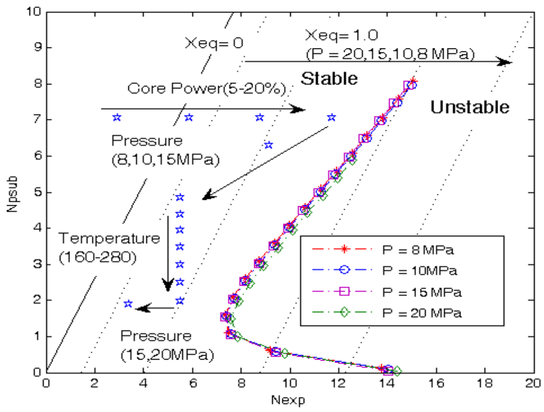

Figure 13 stability analyses for new Pressurization Phase

5. Conclusions

The sliding pressure startup procedures and startup plant systems for CANDU-SCWR are investigated by using subchannel code ATHAS. The stability is also investigated by linear frequency domain method. The startup procedures can be divided into five phases: (1) Start of Reactor Core at Subcritical Pressure; (2)Start of Turbine; (3) Pressurization Phase; (4) Feedwater Temperature Increasing Phase; and (5) Core Power Increasing Phase. The calculation results show that during these phases, the maximum cladding temperature satisfies well the criterion and it also adapt the stability remand. So the proposed sliding pressure startup procedure is feasible in CANDU-SCWR from both thermal hydraulic and stability considerations.

6. References:

[1] Heusener G,Müller U,Schulenberg T,Squarer D. A European development program for a high performance lightwater reactor (HPLWR). Proceedings of SCR-2000. Tokyo, 2000: 23–28.

[2] Duffey R,Pioro I,Khartabil H. Supercritical water-cooled pressure channelnuclear reactors: review and status. Proceedings of GLOBAL 2005. Tsukuba, Japan, 2005.

[3] Nakatsuka T,Oka Y,Koshizuka S. Startup thermal considerations for supercritical-pressure light water-cooled reactors. Nuclear Technology. 2001,221.

[4] Yi TT,Ishiwatari Y,Koshizuka S,Oka Y. Startup Thermal Analysis of a High-Temperature Supercritical-Pressure Light Water Reactor. Journal of Nuclear Science and Technology. 2004,790-801.

[5] Zhao J. Stability Analysis of Supercritical WaterCooled Reactors. Cambridge: Massachusetts Institute of Technology, 2005.

[6] S.Kakac,B.Bon. A Review of two-phase flow dynamic instabilities in tube boiling systems. International Journal of Heat and Mass Transfer. 2007,21,399-433.

[7] Yi TT,Ishiwatari Y. Thermal and Stability Considerations of Super LWR during Sliding Pressure Startup. Journal of NUCLEAR SCIENCE and TECHNOLOGY. 2005,42,537-48.

[8] Shan JQ,Zhang B,Li CY,Leung LKH. SCWR subchannel code ATHAS development and CANDU-SCWR analysis. Nuclear Engineering and Design. 2009,1979-87.

[9] Ishii M,Zuber N. Thermally Induced Flow Instabilities in Two Phase Mixtures. 4th International Heat Transfer Conference. Pari, 1970: Paper No. B 5.11.

[10] Yang P,Cao LZ,Wu HC. Conceptual design of CANDU-SCWR with thermal-hydraulics coupling. Proceedings of the 18th International Conference on Nuclear Engineering. Xi'an, 2010.